JOURNAL OF MATERIALS SCIENCE 25 (1990) 445–454

Development of microstructure in laser surface alloying of steel with chromium

NARENDRA B. DAHOTRE
Center for Laser Applications, The University of Tennessee Space Institute, Tullahoma, Tennessee 37388, USA

K. MUKHERJEE
Department of Metallurgy, Mechanics and Materials Science, Michigan State University, East Lansing, Michigan 48824, USA

Laser surface alloying (LSA) was used to form *in situ* Fe–Cr–C alloys on AISI 1018 steel substrates. Chromium powders of different particle sizes were mixed together to obtain optimum packing density of the powder deposited on the substrate. The surface was then melted using a 2 kW CW carbon dioxide laser. The processing conditions were related to solute (chromium) content, microstructural refinement of the laser alloyed zone and the heat affected zone (HAZ). The microstructure of the laser surface alloyed region was investigated by optical, scanning and transmission electron microscopy, and X-ray microanalysis techniques. Microstructural study showed a high degree of grain refinement and an increase in solid solubility of alloying element. This process produced a fine distribution of complex type of carbide precipitate in the martensite–ferrite matrix because of the high cooling rate. An alloy of this composition does not show any retained phase. The nature of alloying and chemical diffusion profile as a function of intertrack separation distance affects the final content of alloying element in the surface layer.

1. Introduction

In many military and civilian applications, surface degradation by corrosion or erosion is a limiting factor in the effective service life. Often, the surface of a hardware stands between a hostile environment and the interior of the material. For metallic materials, even pure water and oxygen are hostile environments. Such chemically hostile environments give rise to corrosion, stress corrosion cracking or corrosion fatigue in metallic components. Mechanically hostile environments such as impingements of dust particles, abrasive forces against hard surfaces such as sand, gravel or boulders give rise to surface wear, surface cracks and surface fatigue etc. These chemical and mechanical degradations of metallic surfaces can be minimized by various means such as organic coating or painting, designing the entire hardware with a corrosion and erosion resistant material and cladding, metallizing or surface alloying. Whilst coating or painting can provide a protection against corrosion, they have very little effect, if any, in improving the mechanical properties of the surface. The second option, i.e. designing the entire structure with a high strength and corrosion resistant metal or alloy, is economically and strategically unrealistic in most cases. Thus improvements of the surface layer properties by cladding or metallizing is a more realistic approach. It is in this area that laser surface alloying has the most potential. It is also a very promising field for large scale commercial applications.

Laser alloying is a material processing method which utilizes the high power density available from focused laser sources to melt metal coatings and a portion of the underlying substrate. Since the melting occurs rapidly and only at the surface, the bulk of the material remains cool, thus serving as an infinite heat sink. Large temperature gradients exist across the boundary between the melted surface region and the underlying solid substrate, which results in rapid self-quenching and resolidification. What makes laser surface alloying both attractive and interesting is the wide variety of chemical and microstructural states that can be retained because of the rapid quench from the liquid phase. These include chemical profiles where the alloyed element is highly concentrated near the atomic surface and decreases in concentration over shallow depths (hundreds of nanometres), and uniform profiles where the concentration is the same throughout the entire melted region. The types of microstructures observed include extended solid solutions, metastable crystalline phases and metallic glasses.

The present work uses the laser surface alloying (LSA) technique to form *in situ* Fe–Cr–C alloys on AISI 1018 steel substrates on which a mixture of chromium powder of different particle sizes was deposited prior to laser treatment. The microstructure in laser surface alloyed region was characterized by using optical, scanning and transmission electron microscopy and X-ray microanalysis techniques.

0022–2461/90 $03.00 + .12

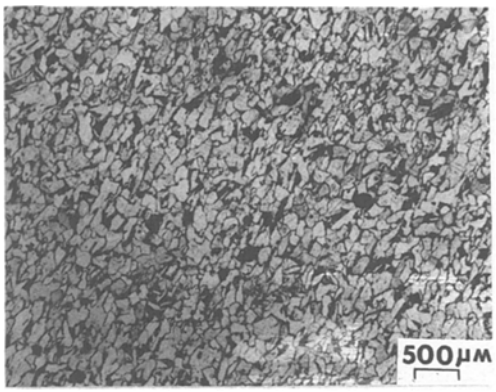

Figure 1 Microstructure of AISI 1018 steel before laser treatment.

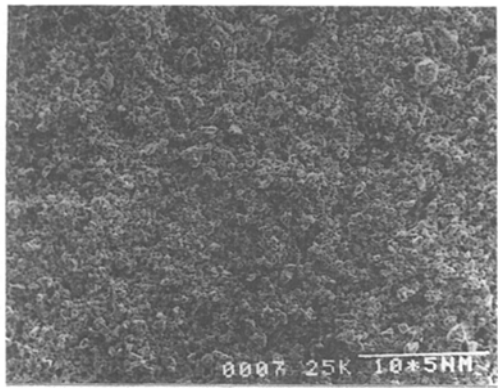

Figure 3 Surface layer of chromium powder of mixture of different particle sizes.

2. Experimental procedure

AISI 1018 steel (0.15 to 0.20 wt % C, 0.6 to 0.9 wt % Mn, 0.04 wt % P and 0.05 wt % S) samples in the shape of a rectangular slab (2.5 cm × 1.25 cm × 1.25 cm) were used for this study. The specimens were annealed at 450° C for about 1 h. The specimens were mechanically polished and then etched in 3% nital to reveal the prior microstructure (Fig. 1). Chromium powder (electrolytic grade with 99.8% purity) was used for alloying purposes. In order to maximize the powder packing density, powder of average particle sizes 40 and 60 μm in the proportion of 3 : 1 by weight were mixed together. The packing factor obtained this way was approximately 0.30. A slurry of chromium in a suitable organic binder was made and a uniform layer was applied onto the specimen surface. The organic binder was allowed to set before laser irradiation. During laser irradiation, organic binder evaporates and powder particles are free to infiltrate into the base metal.

The specimens were mounted on an electrically driven x–y table and irradiated with a continuous wave CO_2 laser beam of 10.6 μm wavelength at a power level of 1500 to 2000 W (schematic is shown in Fig. 2). Argon gas was directed on the sample coaxial with a laser beam to avoid surface contamination. The beam was focused at the surface of the specimen to obtain a spot size of 0.2 mm. The specimen travel speed employed in the study was 8 cm min^{-1}. Several laser tracks in one direction parallel to each other were made. The intertrack spacing was maintained as 2, 1 and 0.5 mm, respectively. One group of samples was also treated with two sets of parallel tracks at right angle to each other. For this case, in both directions the centre to centre distance between successive passes was 0.5 mm.

For optical microscopy observation of laser melted region, an etching reagent consisting of 60 ml H_2O, 40 ml HCl and 10 ml HNO_3 was used. The microhardness measurements were done with a 900 g load. Concentration of elements in the alloyed surfaces were determined by electron microprobe analyser and a field emission scanning transmission electron microscope (FE-STEM). The FE-STEM was operated at 100 kV. Microstructural investigations of laser alloyed surfaces were carried out by optical microscope, scanning electron microscope (SEM) and transmission electron microscope (TEM). The TEM was operated at 200 kV.

The samples were prepared for TEM and FE-STEM observations from laser alloyed region by cutting out 0.3 mm thick wafers parallel to the treated surface (x–y plane, see Fig. 2) on a diamond wheel cutting machine. After mechanically polishing to a thickness of 0.15 mm, 3 mm in diameter discs were punched from the wafers. Finally these discs were thinned in a solution containing 950 ml acetic acid and 50 ml perchloric acid with an applied voltage of 52.5 V at 25° C using a twin jet polisher, for final observations.

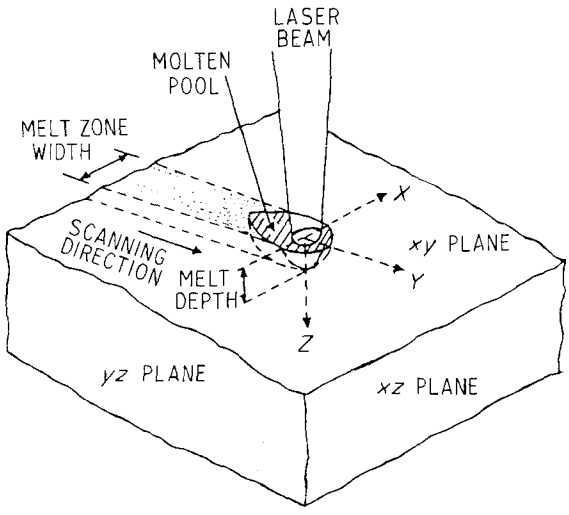

Figure 2 Schematic illustration of laser beam, substrate geometry and coordinate system.

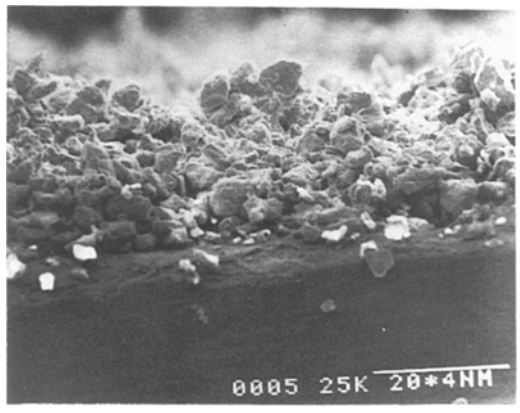

Figure 4 SEM micrograph showing chromium powder layer thickness in cross-section.

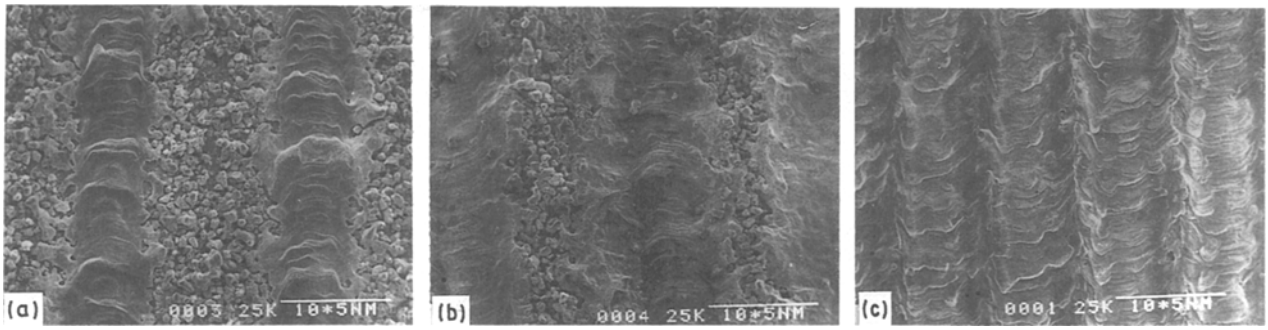

Figure 5 Top view of a laser surface alloyed AISI 1018 steel, with the distance between centre to centre of two successive passes equal to (a) 2 mm, (b) 1 mm and (c) 0.5 mm.

3. Results and discussion

3.1. Topographical features

An optical micrograph of AISI 1018 steel, after annealing and before laser treatment, is seen in Fig. 1. The microstructure consists of uniform grains of pearlite and ferrite. A surface layer of chromium powder is shown in Fig. 3. From micrographs such as this, an analysis of packing density of powder and pores can be made. The chromium powder layer thickness is illustrated in a SEM micrograph in Fig. 4. This thickness is about 0.3 mm. The SEM micrographs in Figs 5a, b and c show evidence for the rippled topograph in a laser track which has been the object of considerable attention by other investigators [1, 2]. As these intertrack distances become smaller, more surface area is melted. It is evident from Fig. 5c that for 0.5 mm centre to centre distance between two successive tracks, the melted regions nearly overlap and a complete surface melting occurs. The appearance of the surface of the sample, in which the laser tracks were made in two perpendicular directions (0.5 mm centre to centre distance) is seen in Fig. 6. The ripple marks correspond to the second set of tracks. In this treatment also, the successive passes are overlappd in both directions ensuring complete melting of surface area.

From Figs 5c and 6, it is quite clear that porosity is developed in the solidified region. Presence of cracks in this solidified region is also a predominant feature as observed in these micrographs and also in Fig. 7 which is a magnified view of the region in Fig. 6. Porosity and cracks are especially concentrated in the area where two successive laser passes overlap. This area basically is the heat affected zone (HAZ) next to the fusion line for both successive passes. This narrow HAZ is the most vulnerable part of the area surrounding the fusion zone [3]. The micro-distribution of alloy elements take part in this region [4]. It has also been concluded earlier [5] that there is a very high vacancy concentration and vacancy clusters in this region. A high concentration of vacancies and subsequent coalescing could provide sites for initiation of cracks in this region.

3.2. Microstructure, hardness and diffusion

Typical cross-sectional views of laser alloyed specimens after surface grinding (x–z plane in Fig. 2) are shown in Fig. 8. As the depth to which these specimens were ground was not the same, it is not possible to compare the melt depths in them. These cross-sectional views, however, represent the microstructural changes which occurred during laser processing. The etching reagent, nital, could not reveal the structure in fusion zone. The region surrounding the fusion zone, in all cases, is essentially martensitic in nature. A comparison of structures in Fig. 8 also shows the extent of spread of this newly formed martensite region around the fusion zone deep into the base metal. The band width of this solid-state transformation around the fusion zone in the above four laser treatments was measured to be 1.3, 1.5, 2.9 and 3.8 mm, respectively. These measurements give an idea of the heat penetration into the substrate as well as the level of temperature developed at different locations. As the intertrack spacing decreases, the gap between martensite region neighbouring fusion zones is bridged (Fig. 8b).

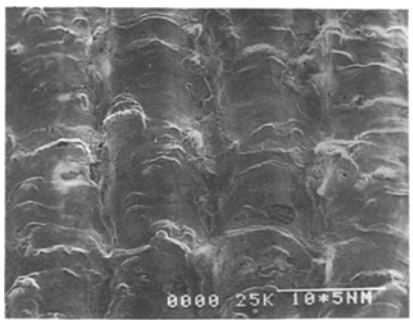

Figure 6 The appearance of surface of the sample in which the laser passes were made in orthogonal directions (centre to centre distance between successive passes is equal to 0.5 mm).

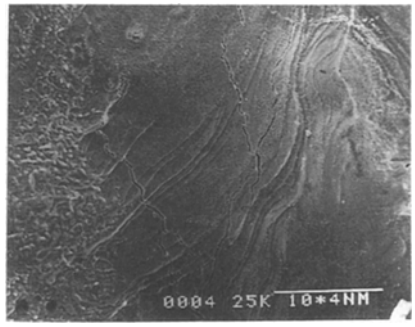

Figure 7 SEM micrograph illustrating concentration of porosity and cracks in the area where two successive laser passes overlap.

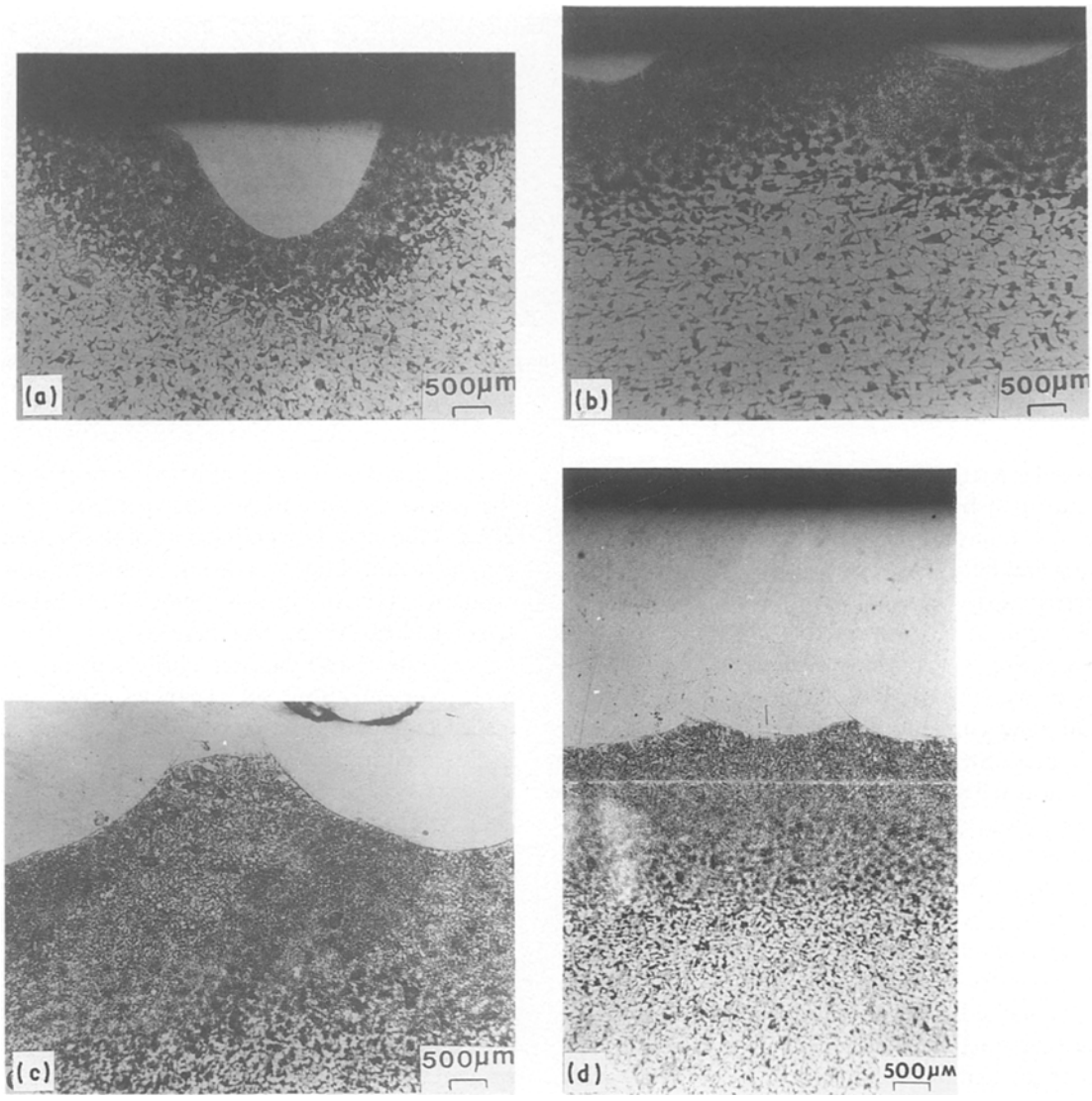

Figure 8 Cross-sectional views of laser alloyed AISI 1018 steel samples after surface grinding. Centre to centre distance between two successive passes is (a) 2 mm, (b) 1 mm, (c) 0.5 mm and (d) 0.5 mm in both orthogonal directions.

In the case of very close laser tracks, in addition to the martensite region, the fusion zones are also bridged (Fig. 8c). Finally, for the two sets of overlapping orthogonal passes, two distinct uniform layers of alloyed zone followed by a solid state transformed martensite region (Fig. 8d) were produced. The heterogeneity of microstructure in the form of bands of martensite observed in HAZ in some specimens (Figs 8b, c and d) may result from local variations in composition. Microstructural heterogeneities of various forms have previously been reported in laser treated material [7, 8]. Such features have been interpreted in terms of factors such as compositional differences due to incomplete solution of phases, dependence of crystal growth direction on thermal gradients and differences in cooling rate.

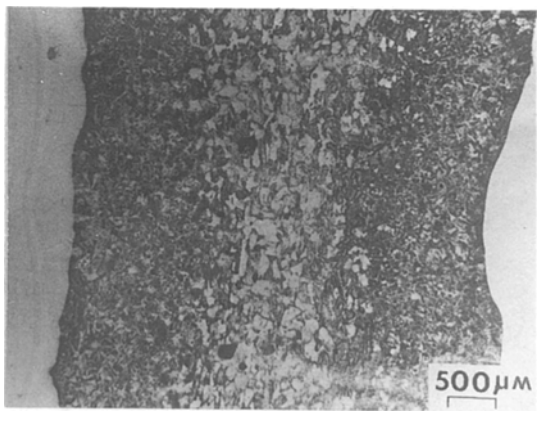

Figure 9 Microstructure in the region between two successive laser passes spaced at about 2 mm apart.

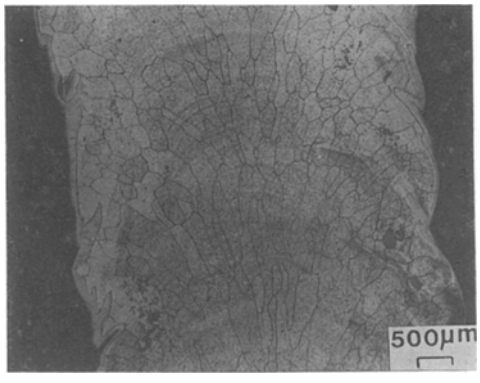

Figure 10 Micrograph showing the cellular grains along traverse direction in fusion zone.

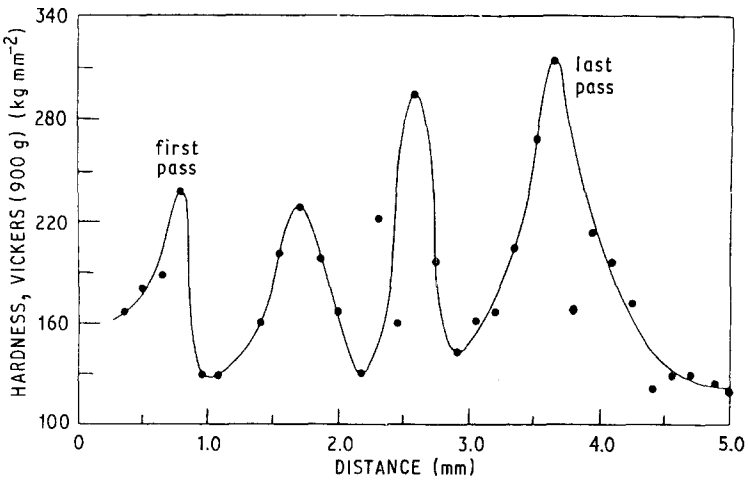

Figure 11 Microhardness profile of chromium surface alloyed AISI 1018 steel, across the surface as a function of distance (x–y plane). The centre to centre distance between two successive passes was 1 mm.

The views of an alloyed surface after surface grinding (x–y plane in Fig. 2) are shown in Figs 9 and 10. The sample in Fig. 9 was etched with nital. It delineates the microstructure in the region between two successive passes at about 2 mm apart. The martensitic structure next to each fusion zone separated by the region of pearlite in ferrite matrix is indicative of substantial variation of cooling rate in this region. The microstructure in the alloyed region was revealed by etching the specimen with 60 ml H_2O, 40 ml HCl and 10 ml HNO_3 which is generally used for stainless steel samples. It illustrates cellular structure (Fig. 10) developed along the traverse direction.

The structural heterogeneities observed in both solidified and solid state transformed (HAZ) regions are the reasons for the very large fluctuations in the value of microhardness across the surface alloy (Fig. 11). This variation is due to the presence of a very fine duplex microstructure consisting of metastable phases and carbide precipitates in alloyed region. It is also evident from Fig. 11 that the highest value of hardness in each fused region drops successively from the last track to the first track. The drop in hardness value is due to the tempering action by the heat supplied by following laser tracks. The extent of tempering and hence the level of the highest value of hardness in a track depends upon the number of following passes. The uniform hardness (DPN 230) was obtained on the surface alloyed by two sets of orthogonal laser passes. Fig. 12 is the hardness traverse on the cross sectional surface (x–z plane in Fig. 2). The hardness value drops across the laser melted–HAZ interface and finally reaches the value of hardness (DPN 135) of the base metal.

The relative diffusion profile of laser alloying elements as a function of intertrack distance was studied. Fig. 13 shows a set of electron microprobe traces across the surface alloy (x–y plane in Fig. 2). This figure shows that the average chromium content in the laser melted region is uniform. As the intertrack spacing decreases, more chromium diffuses into the HAZ surrounding fusion zone (Figs 13a and b). This solid state diffusion deep into the heat affected region, is due to the interaction of heat flow along the surface from successive laser passes. When laser tracks are laid almost overlapping each other in one direction, the chromium content in the surface is about 40 wt % (Fig. 13c). For the same powder thickness, laser power and traverse speed, if the sample is treated for two sets of orthogonal laser passes, almost overlapping in each direction, then the chromium content in surface layer drops by about 70% (to about 12 wt %) as observed in Fig. 13d. Due to two sets of multiple laser passes, the base metal is melted to a greater depth and also the heat diffuses to deep below the surface thereby distributing the same amount of chromium over a large volume of the base metal.

3.3. Structural analysis of laser surface alloyed region

A transmission electron microscopic investigation of the laser surface alloyed region indicated that the

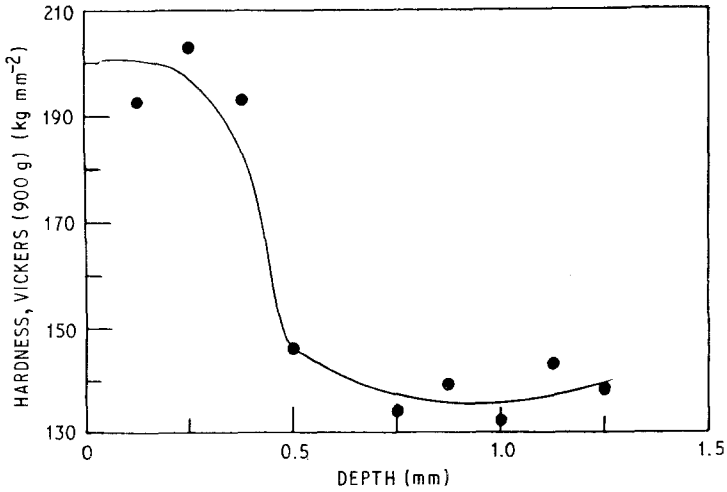

Figure 12 Microhardness profile on cross-sectional surface of chromium surface alloyed region, as a function of distance (x–z plane). The centre to centre distance between two successive laser passes was 0.5 mm in both orthogonal directions.

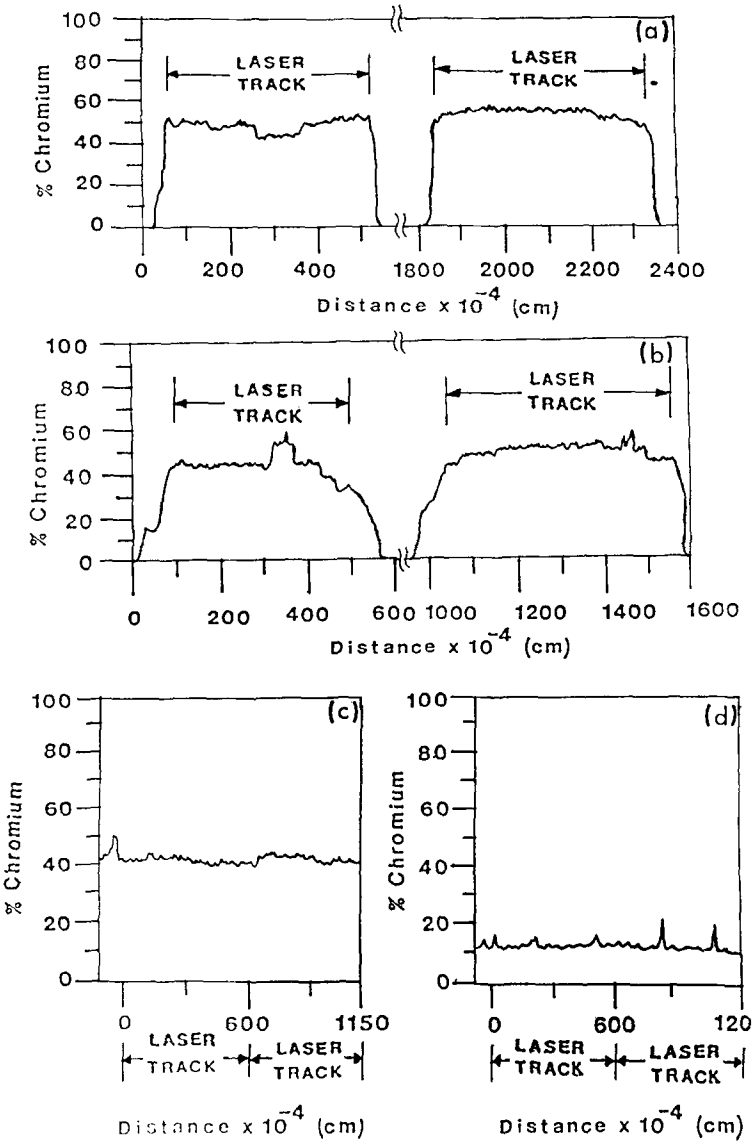

Figure 13 Electron microprobe tracers taken across the surface alloy in a sample treated with laser having centre to centre distance between two successive passes equal to (a) 2 mm, (b) 1 mm, (c) 0.5 mm and (d) 0.5 mm in both orthogonal directions.

microstructure consists of three microstructurally distinct regions: elongated, blocky and matrix as shown in Fig. 14. The TEM micrograph in Fig. 15a illustrates that the elongated microstructure consists predominantly of lath martensite. The structure of the lath martensite consists of a high density of dislocations. As suggested by Kelly and Nutting [9], the addition of chromium to a steel lowers the M_s temperature and also lowers the stacking fault energy thereby producing martensite with a dislocation substructure instead of a twinned one.

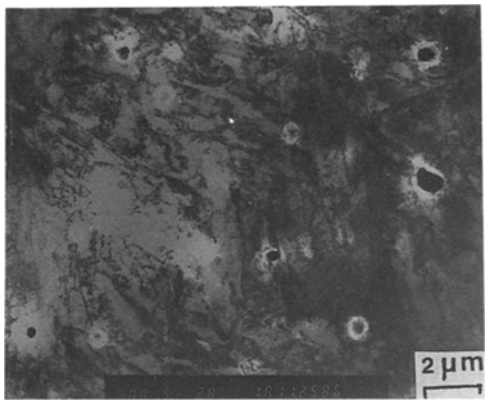

Figure 14 TEM micrograph of the laser surface alloyed region showing three phase structure.

The crystal structure of lath martensite is usually b c c in low-carbon steels [10]. This is probably because of the segregation of carbon atoms to dislocations during quenching. In the present LSA processed samples, on the basis of diffraction analysis, as seen in Figs 15b and c (with [0 0 1] zone axis) and Figs 16b and c (with [$\bar{1}$ 1 1] zone axis), the martensite structure was b c c. The lattice parameter of b c c martensite calculated from this analysis was found to be 0.315 nm. Iron-based martensites that contain only substitutional alloying elements (Fe–Ni, Fe–Ni–Cr) usually have b c c crystal structure because the substitutional alloying elements are distributed at random on the lattice sites [10].

In addition to this martensite structure, the LSA region also contains block type precipitates as observed in Fig. 17a. These precipitates are generally irregular in shape and their size varied from 0.3 to 1.6 μm. Such a large difference appeared due to differences in alloy composition and cooling rates. The precipitates have been identified as $M_{23}C_6$ type with f c c crystal structure as suggested in the literature [11]. This analysis was based on selected area diffraction (SAD) pattern obtained for one of the precipitates and

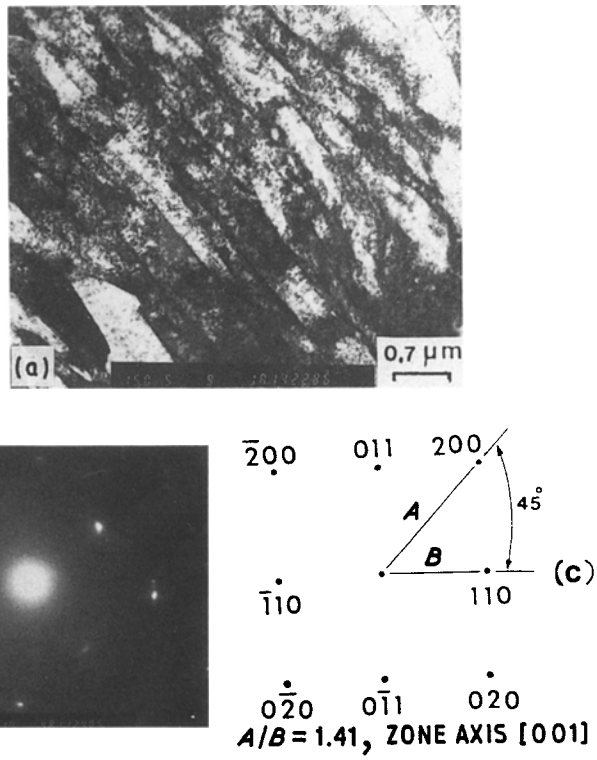

Figure 15 TEM micrographs of the laser surface alloyed region showing martensitic structure. (a) a bright field image, (b) an SAD pattern from (a), and (c) a schematic diagram of the SAD with [0 0 1] zone axis.

is shown in Figs 17b and c. The corresponding STEM X-ray microchemical analysis (Fig. 18) from these precipitates is essentially rich in chromium content with partial substitution of chromium by other metals like iron. Therefore, the carbide precipitates had the $(Cr, Fe)_{23}C_6$ type structure. These precipitates contain a high density defects. These defects appear to be closely space stacking faults. The high resolution bright field TEM of the carbide precipitate shows a regular array of parallel lattice fringes (Fig. 19). The lattice spacing between fringes is approximately 35 nm. Similar kind of fringe pattern was observed in M_7C_3 and M_6C [12] carbide precipitates obtained in laser clad Fe–Cr–Mn–C alloy.

The parallel investigations of the laser surface alloyed region were carried out by a X-ray diffraction technique. The reflections obtained from the as-laser-treated surface (Fig. 20a) were indexed in terms of oxides [$(Cr, Fe)_2O_3$, Fe_3O_4], carbides [$(Cr, Fe_{23}C_6$, $(Cr, Fe)_7C_3$] and Cr-ferrite. The formation of oxides may well be due to strong melt-environment interactions. X-ray diffractometric analysis of the laser treated surface after lightly polishing ($\approx 70\,\mu m$), showed ferrite (α), martensite (α'), carbide [$(Cr, Fe)_{23}C_6$] and

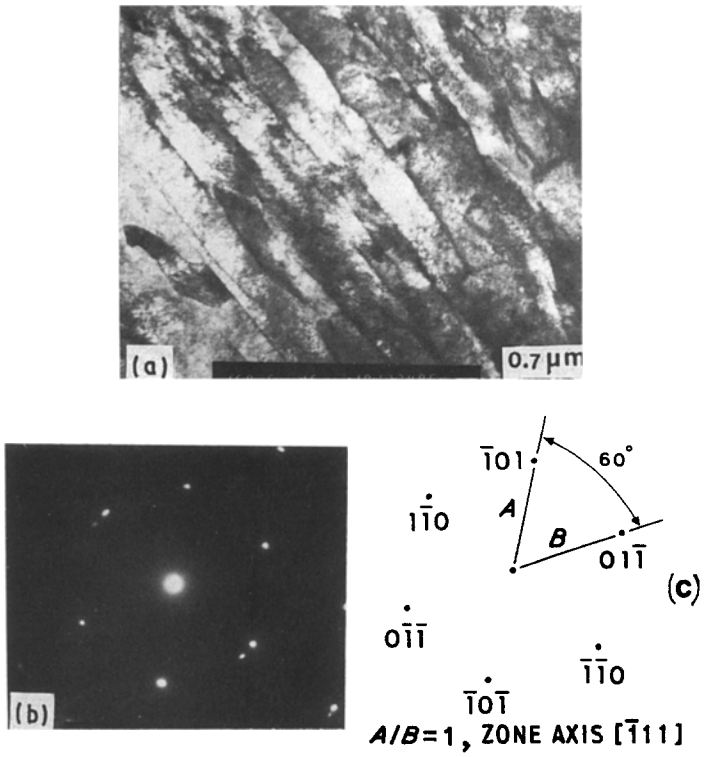

Figure 16 TEM micrographs of the laser surface alloyed region showing martensitic structure. (a) a bright field image, (b) an SAD pattern from (a) and (c) a schematic diagram of the SAD with [$\bar{1}$ 1 1] zone axis.

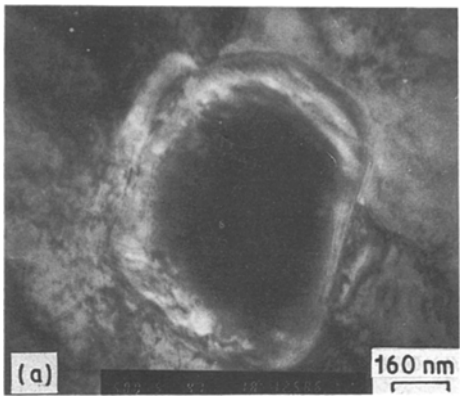

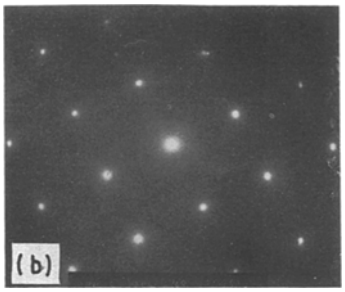

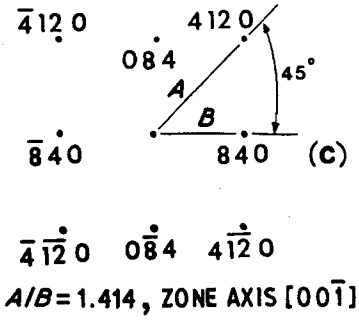

Figure 17 TEM micrographs of the laser surface alloyed region showing $M_{23}C_6$ type carbide. (a) a bright field image, (b) an SAD pattern from (a) and (c) a schematic diagram of the SAD.

some traces of oxide [$(Cr, Fe)_2O_3$] (Fig. 20b). The disappearance of other kinds of carbides $(Cr, Fe)_7C_6$, is attributed to cooling rates present in this region. At the surface, an extremely rapid solidification process and higher content of chromium and carbon introduces a non-equilibrium phase such as $(Cr, Fe)_7C_3$. However, in both the above cases a few reflections remain unaccounted for.

On the basis of above mentioned microstructural analysis and ternary Fe–Cr–C system phase diagram (Fig. 21), [10] possible phase transformation sequence could be presented as follows

$$L \rightarrow L + \alpha \rightarrow (\alpha + \alpha')_I + L$$
$$\rightarrow (\alpha + \alpha')_I + (\alpha + M_{23}C_6)_{II}$$

where L is the liquid. It appears from the above sequence that the first transformation products (I) are ferrite α, and martensite α', followed by the formation of $M_{23}C_6$ along with ferrite. Such unconventional transformations are often found in the rapid solidification process (RSP).

Several explanations are given for the formation of phases in an unconventional manner in the rapid solidification process such as that mentioned above. According to some researchers [13] the rapid solidification process can produce large undercoolings below liquidus temperature. When this occurs solidification takes place without diffusion. Considering the Fe–Cr–C system it is likely that an undercooling would be sufficient for formation of austenite which, finally due to an extremely high rate of cooling, transforms to martensite. Whereas, according to Molian *et al.* [14], in laser processed Fe–30% Cr–0.2% C (all wt%) surface alloy, at high cooling rate the phases like ferrite and martensite are unable to reject substantial amounts of solute atoms such as chromium and carbon. Therefore, the remaining excess amount of

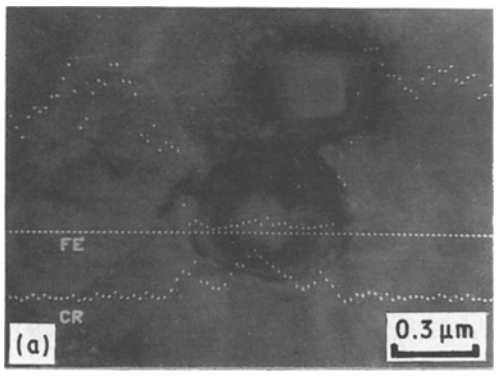

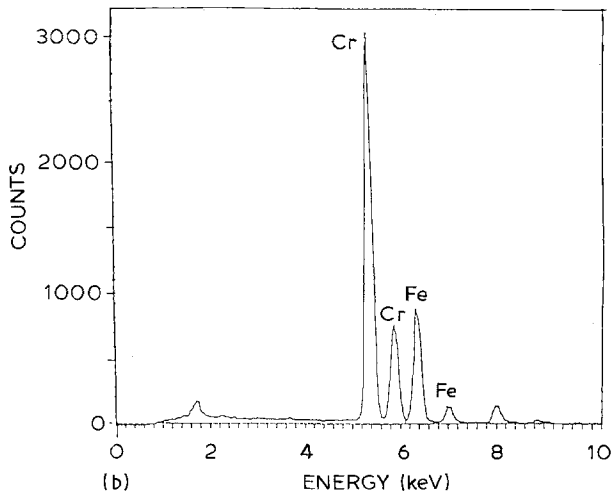

Figure 18 STEM X-ray microchemical analysis of (a) the laser surface alloyed region and (b) the $M_{23}C_6$ type carbide precipitate.

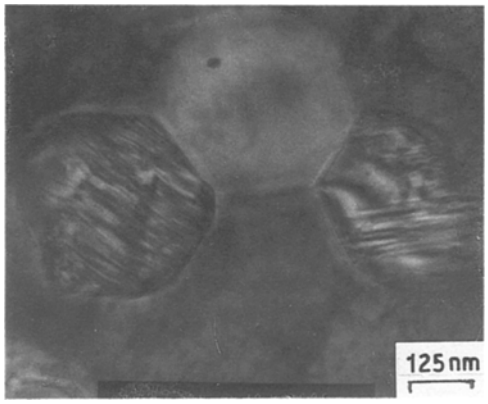

Figure 19 High resolution transmission electron micrograph of laser alloyed region showing $M_{23}C_6$ carbide precipitate.

chromium and carbon would be rejected by the non-equilibrium phases into the remaining melt which becomes supersaturated and forms a deep eutectoid. Again because of high cooling rates, fcc carbide $M_{23}C_6$ type would be formed which is an equilibrium carbide precipitate. This explanation is based upon the assumption that $M_{23}C_6$ carbides are formed from the melt.

At this juncture, another possible explanation for formation of $M_{23}C_6$ carbide is that it could be through a solid state transformation. In this LSA process, several overlapping passes were laid on the material. The temperature developed at laser beam–metal interaction is sufficiently high to raise the temperature of the surrounding region by several hundreds of degrees. Thus solidified and alloyed region due to previous passes undergoes a tempering treatment. In low carbon alloy steel cementite and carbides formed during solidification are dissolved during tempering and a sequence of alloy carbides are formed [10]. Similarly, in present LSA process, $M_{23}C_6$ type carbides may have been formed from cementites and other type of carbides due to tempering. The formation of alloy carbides in this manner is sometimes referred to as secondary hardening [10].

4. Conclusion

A laser surface alloyed Fe–Cr–C alloy produced a very fine grain microstructure of ferrite, lath martensite and complex carbide ($M_{23}C_6$) precipitation. The substructure of martensite was dislocated and the crystal structure of martensite was bcc. The increase in solid solubility and high cooling rate first produced martensite along with high temperature ferrite followed by the formation of $M_{23}C_6$ (fcc) carbide precipitate. The $M_{23}C_6$ carbide precipitates were uniformly distributed in the matrix which had a high content of

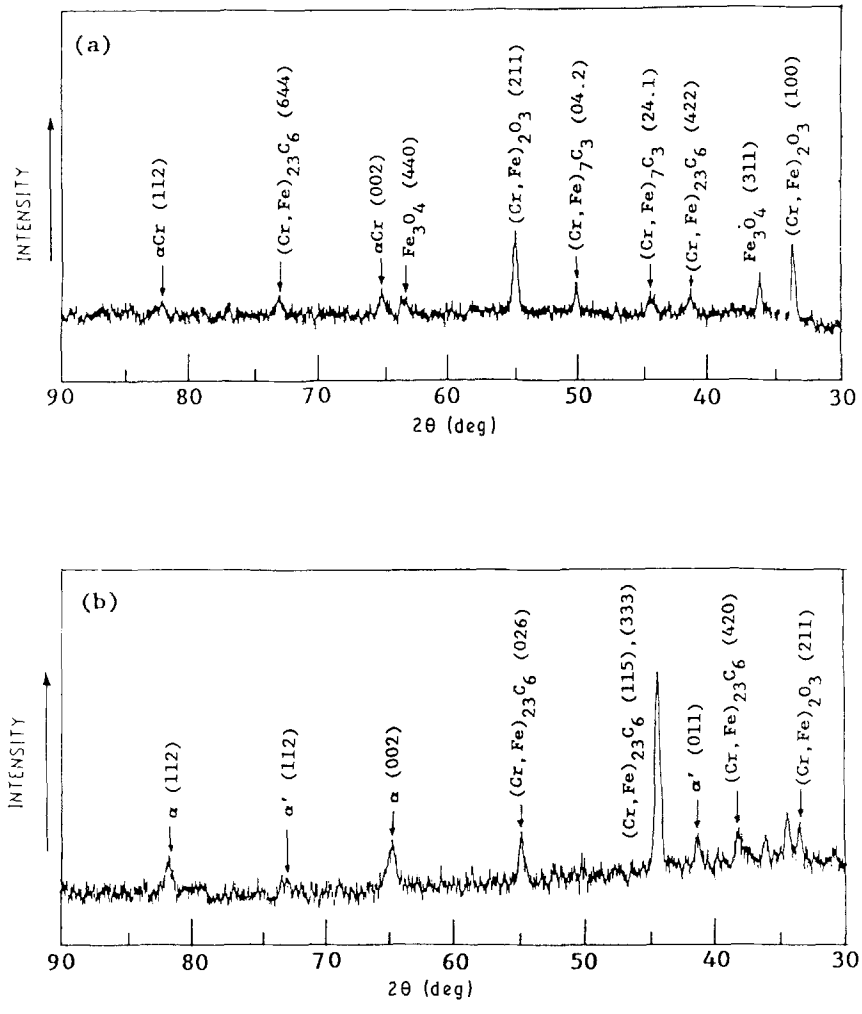

Figure 20 X-ray diffractometry data from laser surface alloyed region. (a) as-laser-treated and (b) after lightly polishing the laser alloyed surface.

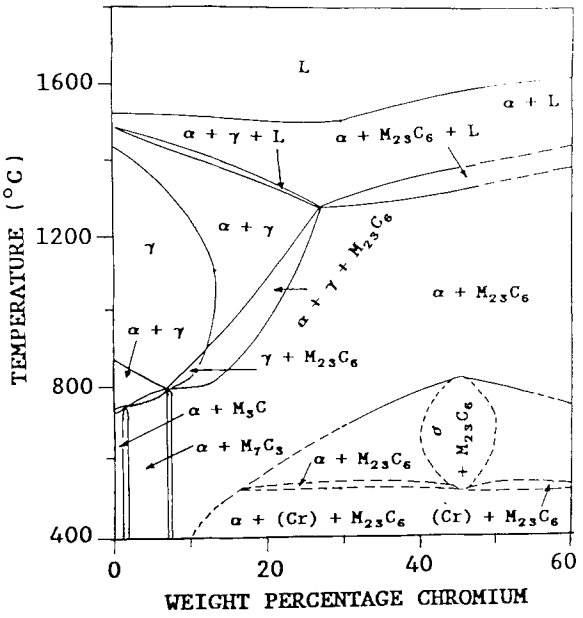

Figure 21 A cross-sectional diagram for Fe–Cr–C system containing 0.1% carbon.

chromium. The defects such as porosity and cracks are produced during laser surface alloying.

References

1. T. R. ANTHONY and H. E. CLINE, *J. Appl. Phys.* **48** (1977) 3888.
2. S. L. NARASIMHAN, S. M. COPLEY, E. M. VASTRYLAND and M. BASS, *Met. Trans.* **10A** (1979) 654.
3. N. B. DAHOTRE, A. HUNTER and K. MUKHERJEE, *J. Mater. Sci.* **2** (1987) 403.
4. B. S. KASATKIN and A. M. TSARYUK, *Automatic Welding* **2** (1956) 1.
5. K. MUKHERJEE, T. H. KIM and W. T. WALTER, in "Lasers in Metallurgy" (The Metallurgical Society of AIME, Warrendale, PA, 1981) p. 137.
6. D. ROSENTHAL, *Welding J.* **20** (1941) 2205.
7. Y. W. KIM, P. R. STRUTT and H. NOWOTNY, *Met. Trans.* **10A** (1979) 881.
8. K. LIPSCOMBE, W. M. STEEN and D. R. F. WEST, in "Rapid Solidification Processing: Principles and Technologies II" (Claitors Publishing Division, Baton Rouge, LA, 1980) p. 189.
9. P. M. KELLY and J. NUTTING, *J. Iron Steel Inst.* **6** (1961) 199.
10. Metals Handbook, Metallography, Structures and Phase Diagrams, 8 (ASM, Metals Park, OH, 1973) 202.
11. K. W. ANDREWS, D. J. DYSON and K. R. KEOWN, in "Interpretation of Electron Diffraction Patterns" (Plenum, New York, 1967) p. 197.
12. J. SINGH and J. MAZUMDER, *Met. Trans.* **18A** (1987) 313.
13. M. COHEN, B. H. KEAR and R. MEHRABIAN, in Proceedings of 2nd International Conference on Rapid Solidification Processing, Reston, Virginia, March 1980 (Claitors Publishing Division, Baton Rouge, LA, 1980) p. 1.
14. P. A. MOLIAN, P. J. WANG, K. H. KHAN and W. E. WOOD, in "Materials Research Society Proceedings of Rapidly Solidified Amorphous and Crystalline Alloys", edited by B. H. Kear, B. C. Giessen and M. Cohen, Vol. 8 (North Holland, Amsterdam, 1981) p. 511.

Received 12 December 1988
and accepted 10 April 1989